Numerical Study of the Local Downslope Wind "Hirodo-Kaze" in Japan

HIRONORI FUDEYASU,* TSUNEO KUWAGATA,+ YUKITAKA OHASHI,# SHIN-ICHI SUZUKI,@ YASUTOMO KIYOHARA,& AND YU HOZUMI**,++

*Japan Agency for Marine-Earth Science and Technology, Kanagawa, Japan
+National Institute for Agro-Environmental Sciences, Tsukuba, Japan
#Okayama University of Science, Okayama, Japan
@National Research Institute for Earth Science and Disaster Prevention, Tsukuba, Japan
&Graduate School of Science and Technology, Kobe University, Kobe, Japan
**Acid Deposition and Oxidant Research Center, Nishi-ku, Japan

(Manuscript received 10 October 2006, in final form 16 April 2007)

ABSTRACT

The "Hirodo-kaze," a local strong wind accompanying the downslope winds in Japan, is examined using a mesoscale numerical model. The model successfully reproduces the major features of the observed Hirodo-kaze that occurred in association with Typhoon Pabuk. During the Hirodo-kaze, the severe downslope winds in the transitional flow develop in the lower troposphere below the mean-state critical layer. The Hirodo-kaze is closely linked to the strong wind region accompanying the severe downslope winds. After the cessation of the Hirodo-kaze, distinct mountain waves dominate in the lower troposphere where the Scorer parameter l^2 decreases with height. The region of strong wind retreats windward as the Hirodo-kaze ceases. Temporal changes in the characteristics of mountain waves in the lee of Mt. Nagi are primarily attributed to the changes in the large-scale environmental winds due to the movement of the intense cyclone.

Environmental conditions favorable for the occurrence of the Hirodo-kaze include strong northerlies in the lower troposphere overlain by southerlies in the middle troposphere. The intense cyclone that moves over the sea southwest of the Kii peninsula creates favorable environmental conditions that support the occurrence of the Hirodo-kaze.

1. Introduction

The "Hirodo-kaze" is one of the well-known strong local winds in Japan. Hirodo-kaze occurs at the southern base of Mt. Nagi (1240 m) in the northeastern Okayama Prefecture, Japan (see Fig. 1), when the lower-troposphere synoptic wind is strong northerly in association with an intense cyclone. In a typical case of the Hirodo-kaze, strong northerlies with a maximum wind speed V_{max} (10-min average) exceeding 15 m s^{-1} persist for several hours and cause severe damage locally in areas south of Mt. Nagi. In late June 1998, for example, a Hirodo-kaze with V_{max} of 25 m s^{-1} occurred in association with Typhoon Peter and caused damages of about $1.0 million (U.S. dollars).

Previous studies considered that Hirodo-kaze winds are related to severe downslope winds on the southern slope of Mt. Nagi that are induced by strong lower-tropospheric northerlies accompanying an intense cyclone. Yoshino (1986) suggested that the orographic configuration of Mt. Nagi, a steep southern slope and a gradual northern slope (see Fig. 1), is favorable for the occurrence of a downslope wind on the southern slope of Mt. Nagi. Sahashi (1988) observed a roll cloud parallel to the ridgeline in the south of Mt. Nagi at the day when the Hirodo-kaze occurred in association with Typhoon Freda (1987). He speculated that severe downslope winds of the Hirodo-kaze are associated with a large-amplitude mountain wave with a rotor cloud (Queney et al. 1960; Vosper 2004, 2006). Nakamura et al. (2002) observed two cases of Hirodo-kaze at the crest and southern base of Mt. Nagi. Observational evidence suggested that there is no significant change in

++ Deceased.

Corresponding author address: H. Fudeyasu, Japan Agency for Marine-Earth Science and Technology, Institute of Observational Research for Global Change, JAMSTEC Yokosuka headquarters, 2-15, Natsushima-Cho, Yokosuka-city, Kanagawa 237-0061, Japan.
E-mail: fudeyasuh@jamstec.go.jp

DOI: 10.1175/2007MWR2049.1

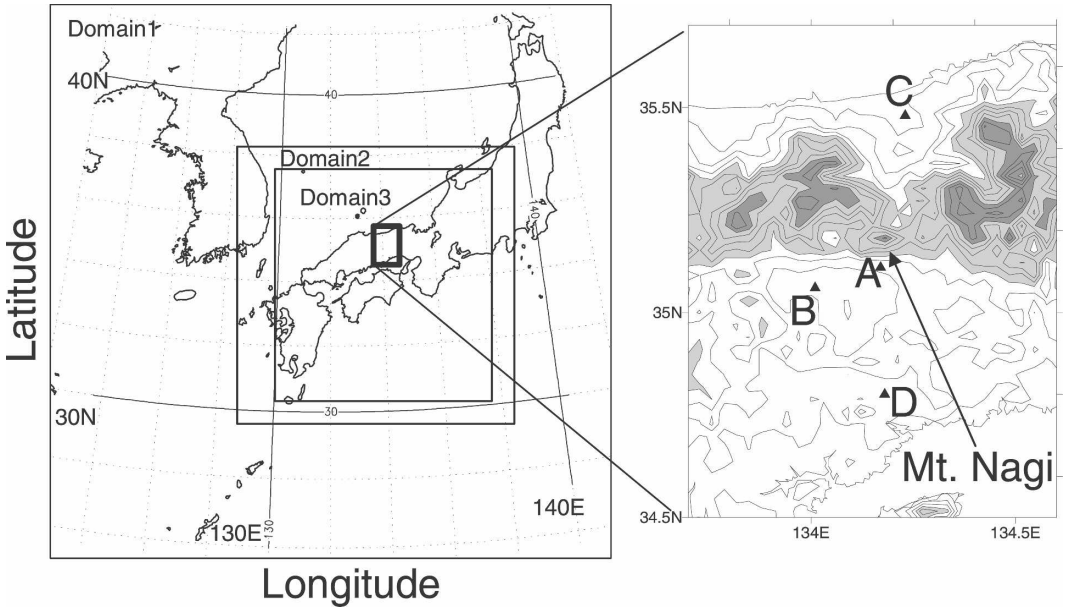

FIG. 1. Model domains of (left) numerical simulations and (right) terrain (contours) around Mt. Nagi. Contour interval is 100 m. Altitudes of 400–800 m are lightly shaded, while altitudes above 800 m are heavily shaded. Triangles show the meteorological stations recording surface wind data shown in Fig. 3.

rainfall and surface temperature accompanied by the Hirodo-kaze, indicating different situation from a bora-like windstorm (e.g., Reed 1981; Smith 1987) and foehn phenomena (e.g., Ikawa and Nagasawa 1989; Furger et al. 2001). Another interesting observational fact is that the Hirodo-kaze ceased, although the northerly at the crest of Mt. Nagi remained strong. The reason for this inconsistency at the cessation of the Hirodo-kaze is not clear. Sahashi (1993) statistically investigated the response of a Hirodo-kaze to the location of a cyclone. A Hirodo-kaze always occurs as an intense cyclone moves northeastward over the sea southwest (offshore) of the Kii peninsula (see Fig. 2). The Hirodo-kaze starts to weaken as the cyclone makes landfall on the Kii peninsula. This relationship between the behavior of Hirodo-kaze and position of an intense cyclone remains unclear.

Severe downslope winds have been observed in mountainous area throughout the world and have been studied using several approaches. Observational studies (e.g., Lilly and Zipser 1972; Doyle and Smith 2003) have described the flow structure of severe downslope winds associated with large-amplitude mountain waves in the lee of mountains. Numerical experiments (e.g., Klemp and Lilly 1975; Clark and Peltier 1977, 1984; Peltier and Clark 1979; Zängl 2002) have suggested that large-amplitude mountain waves are highly nonlinear phenomena, which makes it difficult to apply a linear theory. These studies (e.g., Peltier and Clark 1979; Durran 1986a) revealed nonlinear effects, such as critical-layer reflection mechanisms at a critical layer (layer of zero wind or flow reversal) that acts as a boundary to reflect upward propagating waves back toward the

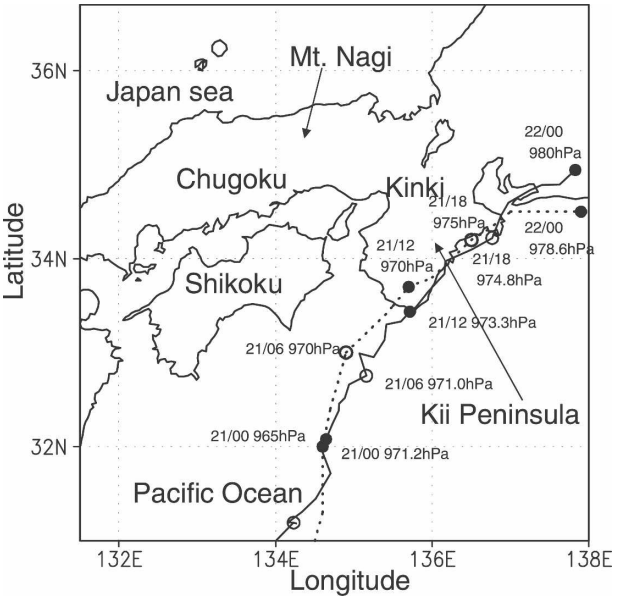

FIG. 2. Track (broken line) of Pabuk from best-track data, compared with simulated Pabuk's track (solid line) derived from domain 3 between 1800 UTC 20 Aug and 0000 UTC 22 Aug 2001. Closed circles represent positions of Pabuk at 0000 and 1200 UTC, while open circles represent positions at 0600 and 1800 UTC.

ground, producing a resonant wave in the lee of the mountain. Smith (1985) solved Long's (1954) equation for nonlinear flow beneath a well-mixed stagnant layer induced by a breaking wave. He obtained a transitional flow, manifested as a severe downslope windstorm, as the mountain flow transitions from an upstream subcritical flow to a downstream supercritical flow. His prediction agreed with numerical results (e.g., Clark and Peltier 1984) and was essential to the application of hydraulic theory (Saito 1992). Results from realistic simulations using a nonhydrostatic mesoscale model have described the details of severe downslope wind (e.g., Saito 1993, 1994; Jackson and Steyn 1994; Doyle et al. 2000). Saito and Ikawa (1991) and Saito (1993, 1994) studied the strong local wind "Yamaji-kaze" in Japan. Their realistic simulations accurately reproduced the severe downslope wind and showed that the Yamaji-kaze was associated with a large-amplitude mountain wave and an internal hydraulic jump. Saito (1993) also discussed the effects of three-dimensional orography on the Yamaji-kaze. Recently, in several case studies, a boundary layer response to wave forcing has been examined by numerical and observational studies (Jiang and Doyle 2005; Jiang et al. 2006, 2007; Vosper et al. 2006).

The studies noted above have described the mechanisms that force severe downslope winds and large-amplitude mountain waves. However, descriptions of the effect of temporal changes in the large-scale environment on the severe downslope wind are scarce. For the case of Hirodo-kaze, a controversial issue includes the response of a Hirodo-kaze to the location of an intense cyclone (Sahashi 1993). Temporal changes in the large-scale environment due to the movement of an intense cyclone are likely a key factor controlling the behavior of a Hirodo-kaze.

The purpose of the present study is to examine the forcing mechanisms during a Hirodo-kaze and the effects of an intense cyclone on the occurrence of a Hirodo-kaze. We used the result of a high-resolution numerical model to invest a Hirodo-kaze that occurred on 21 August 2001 in association with Typhoon Pabuk. In addition, we statistically investigated the effects of the intense cyclone on the occurrence of the Hirodo-kaze. Section 2 of this paper describes observational data and the numerical model used in the study. Section 3 compares structures of the Hirodo-kaze as simulated by the numerical model with observations. Mechanisms forcing the Hirodo-kaze and the dynamic effects of the intense cyclones are discussed in section 4. Finally, results are summarized in section 5.

2. Data and model configurations

a. Data

Data from the Automated Meteorological Data Acquisition System (AMeDAS) were used to identify the spatial and temporal changes in the surface structures of the Hirodo-kaze. The AMeDAS data include surface winds, temperature, and rainfall amounts averaged at a 10-min interval. These data have been available since 1995. Stations A–D, indicated on the right-hand side of Fig. 1, are AMeDAS stations Nagi, Tsuyama, Tottori, and Wake, respectively. Large-scale atmospheric conditions over Mt. Nagi were investigated using the 40-yr European Centre for Medium-Range Weather Forecasts (ECMWF) Re-Analysis (ERA-40) data. These data have a resolution of 2.5° at 6-h intervals.

The plotted track of Pabuk was derived from the best-track archives of the Regional Specialized Meteorological Centers (RSMC) Tokyo–Typhoon Center. The archived dataset includes a cyclone's name, positions, surface pressure, and maximum wind speeds, generally recorded at 6-h intervals.

b. Model configuration

Numerical simulation used the fifth-generation Pennsylvania State University (PSU)–National Center for Atmospheric Research (NCAR) Mesoscale Model (MM5, version 3.5). MM5 is a nonhydrostatic model (Dudhia 1993; Grell et al. 1995) that solves nonlinear primitive equations on Cartesian coordinates in the horizontal and terrain-following sigma coordinates in the vertical.

The numerical simulation was run in the three domains shown in Fig. 1. The outermost domain (D1), centered at 34°N, 132°E, had 200 × 180 grid points with a horizontal resolution of 9 km. The intermediate domain (D2) had 301 × 301 points with a horizontal resolution of 3 km, and the innermost domain (D3) had 700 × 700 points with a horizontal resolution of 1 km. All three domains included 30 vertical layers with fine resolution near the surface, and the top of each model domain was 100 hPa. The model run on D1 produced initial and boundary conditions for the inner domains. The model run on D3 explicitly resolved the fine structure of the Hirodo-kaze.

A simple ice scheme (Dudhia 1989) was used in the model for cloud microphysics. Cloud water and rainwater cooler than 0°C were treated as ice and snow, respectively. The model also included a turbulence parameterization in the planetary boundary layer (Hong and Pan 1996), a five-layer soil model, and a cloud–radiation interaction scheme (Dudhia 1989, 1993; Grell

et al. 1995). A convective parameterization scheme was not used in this simulation.

The initial and lateral boundary conditions for simulation on D1 were derived from the Regional Analysis (RANAL) data and daily mean sea surface temperature (SST) produced by the Japan Meteorological Agency (JMA). The dataset includes the three-dimensional analyses over East Asia. The data have a horizontal resolution of 20 km on 11 vertical layers at 6-h interval.

Simulation on D1 was run for 36 h, starting at 1200 UTC 20 August 2001, after a 12-h model integration from 0000 UTC 20 August using the RANAL that allowed initial spinup. Continuous dynamic assimilation occurred during the initial spinup by adding forcing functions to the governing model equation, which gradually "nudged" the wind components of the model state toward the RANAL (Grell et al. 1995). Lateral boundary conditions used relaxation (Anthes et al. 1987), in which the model-predicted values were relaxed to those estimated from the large-scale analysis. Simulations on D2 and D3 began at 1200 UTC 20 August 2001 and ran for 36 h using initial and boundary conditions interpolated from the results of the outer-domain simulation.

3. Results

a. Features of the observed Pabuk and Hirodo-kaze

Typhoon Pabuk strengthened to a typhoon (maximum 10-min sustained wind speeds in excess of 17.2 $m\,s^{-1}$, or 34 kt) from a tropical depression near the Marshall Islands on 14 August 2001. It recurved over the sea to the south of Japan on 20 August and subsequently approached the Kii peninsula (Fig. 2). Pabuk made landfall on the Kii peninsula at 1200 UTC 21 August with a central pressure of 970 hPa and maximum wind speeds of 30 $m\,s^{-1}$.

At 0600 UTC 21 August 2001, when Pabuk was located over the sea about 80 km southwest of the Kii peninsula, strong surface winds related to the cyclonic circulation of Pabuk were observed in the Shikoku and Kinki districts (Fig. 3). Relatively weak northerlies prevailed in the Chugoku district far from Pabuk, but a strong northerly of 16 $m\,s^{-1}$ was observed at station A located in the lee of Mt. Nagi, about 5 km south of the crest of Mt. Nagi. This strong northerly at station A was a Hirodo-kaze. Winds as strong as the Hirodo-kaze were not observed at stations B, C, and D. The Hirodo-kaze occurred only locally just south of Mt. Nagi.

Figure 4 shows time series of surface wind speed and

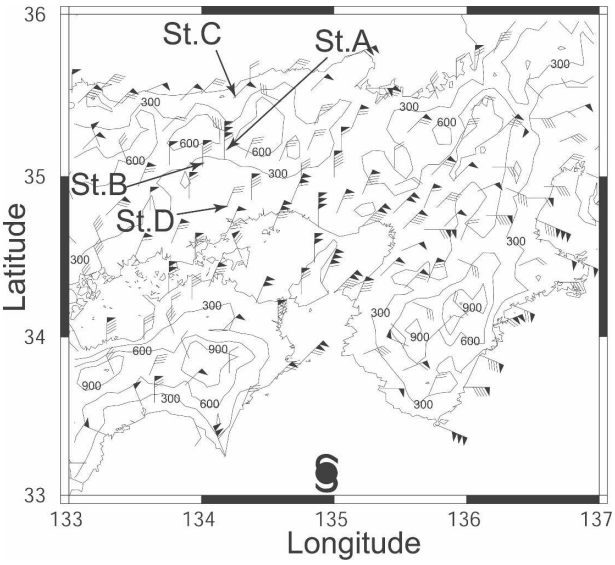

FIG. 3. Surface wind (barbs) and terrain (contours) at 0600 UTC 21 Aug 2001 derived from the AMeDAS data. A full wind barb represents 5 $m\,s^{-1}$. Contour interval is 300 m. The cyclone symbol represents the position of Pabuk.

direction observed at each of the four stations. The Hirodo-kaze was observed only at station A: wind speeds increased between 0100 and 0600 UTC 21 August and then decreased between 1300 and 1800 UTC. Strong northerlies exceeded 15 $m\,s^{-1}$ for about 7 h. Relatively weak northerlies were observed at station B, which was near station A, as the Hirodo-kaze occurred. At that time, weak northerlies were observed at stations C and D, which were windward and leeward of station A, respectively. Southerlies occurred at station A between 1700 and 2100 UTC after the Hirodo-kaze ceased. Southerlies were also observed at station B between 0900 and 1500 UTC. Strong northerlies were recorded at station C between 1500 and 2200 UTC after the Hirodo-kaze ceased at station A. Counterclockwise changes in wind directions (veering) occurred at stations C and D as Pabuk passed, because these stations were to the left of the moving direction of Pabuk. Counterclockwise changes in wind direction at stations A and B were not distinct. No significant change in surface temperature was recorded at station A as the Hirodo-kaze occurred. Weak rain fell at station A during the Hirodo-kaze (not shown). Observational results confirmed that the Hirodo-kaze accompanying Pabuk was a typical Hirodo-kaze.

b. Validation of the simulated Pabuk and Hirodo-kaze

We used observations to validate the simulated results of the Pabuk and the Hirodo-kaze. Figure 2 shows

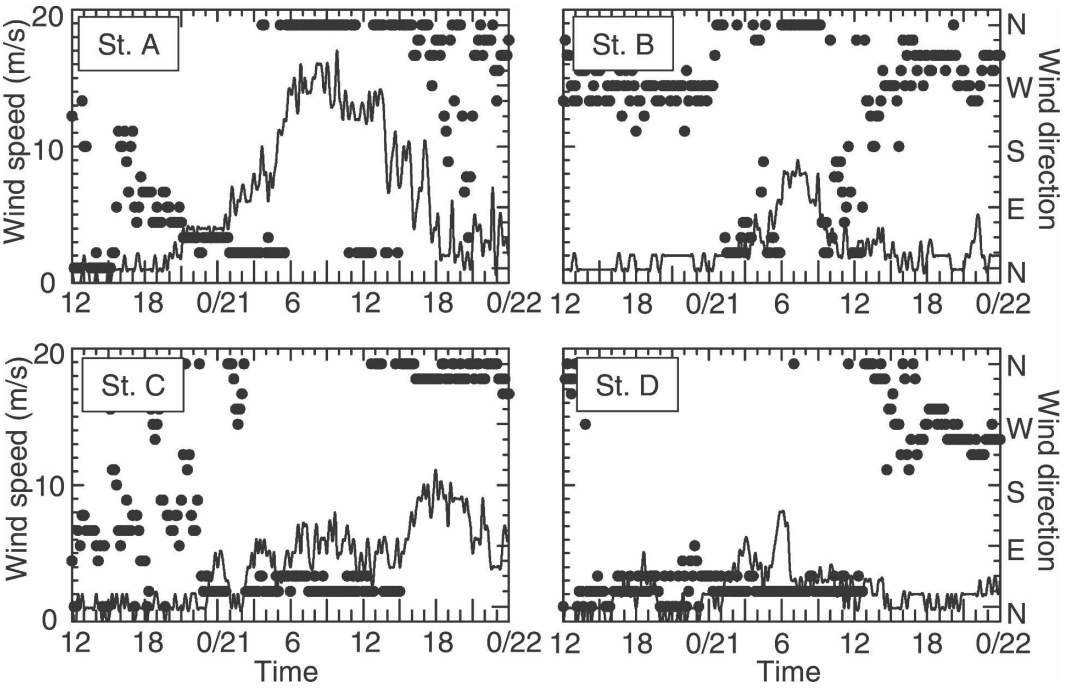

FIG. 4. Time series of surface wind speed (lines) and direction (dots) recorded at meteorological stations during the passage of Pabuk on 20–21 Aug 2001. Station locations are indicated in Fig. 1.

the track of the simulated Pabuk in D3, the run with the finest resolution. The position of the Pabuk's center was determined from the area of minimum sea level pressure in the simulated Pabuk and was in good agreement with the observed track of Pabuk. Central pressures of the simulated Pabuk were about 970 hPa on 21 August. Observed pressures of Pabuk at this time ranged from 965 to 970 hPa. The MM5 reproduced the track and intensity of Pabuk.

Figure 5 shows surface winds at 0600 UTC 21 August 2001 as simulated by D3. A simulated cyclonic circulation prevailed over the Shikoku and Kinki districts. Relatively weak northerlies appeared over the Chugoku district, but simulated northerlies exceeding 15 m s^{-1} appeared near Mt. Nagi. The region of strong winds was 80 km long and 20–30 km wide and extended southwest to the south of Mt. Nagi. Wind exceeded 20 m s^{-1} at station A; simultaneously, winds were less than 10 m s^{-1} at stations B and D. The limited region of strong simulated northerlies south of Mt. Nagi was consistent with observational results (Fig. 3).

Figure 6 shows a time series of simulated surface wind at 10-min intervals at each station. The following simulation results compared favorably with the observations (Fig. 4). The Hirodo-kaze was simulated at station A. Wind speeds increased to near 20 m s^{-1} between 0100 and 0700 UTC and then decreased between 1100 and 1500 UTC. Wind speeds of the simulated Hirodo-kaze were slightly higher than the observed Hirodo-kaze. However, temporal changes in the simulated Hirodo-kaze resembled the observed changes. Relatively weak northerlies appeared at station B as the Hirodo-kaze occurred at station A. Northerlies

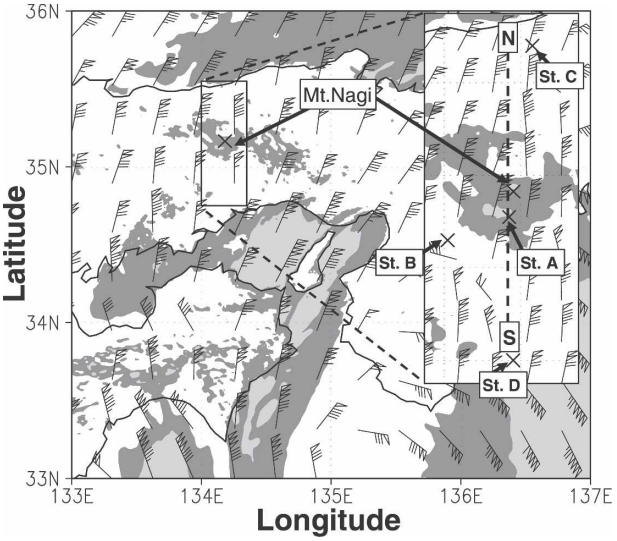

FIG. 5. Simulated surface wind direction and wind speed (barbs) in the large- and local-scale area derived from the simulation in domain 3 at 0600 UTC 21 Aug 2001. A full wind barb represents 5 m s^{-1}. Wind speeds exceeding 15 and 20 m s^{-1} are heavily and lightly shaded, respectively.

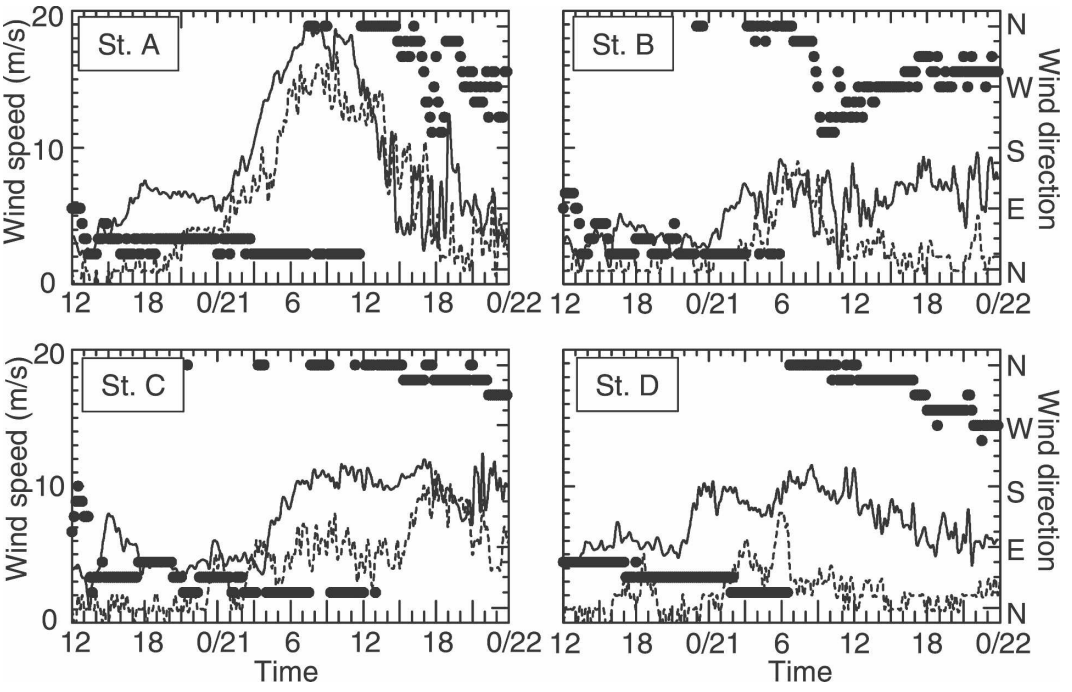

FIG. 6. As in Fig. 4, but for simulated surface wind speed (solid lines), observed wind speed (broken lines), and simulated wind direction (dots).

weaker than the Hirodo-kaze were simulated at stations C and D as the Hirodo-kaze occurred at station A. However, the winds at stations C and D were stronger than observed. Southerlies were simulated at station A between 1600 and 1900 UTC after the Hirodo-kaze ceased. Southerlies were simulated at station B between 0900 and 1300 UTC. Simulated northerlies persisted at station C after the Hirodo-kaze ceased. Counterclockwise changes in simulated wind direction with time were clear at stations C and D, but less distinct at stations A and B. Surface winds simulated at each station agreed well with the observations.

The simulation reproduced major features of the observed Hirodo-kaze. The simulated data could therefore be used with confidence to investigate the vertical structure of the Hirodo-kaze.

c. Structure of the simulated Hirodo-kaze

The structures of the simulated Hirodo-kaze are examined in this section. Figures 7–9 show vertical cross sections of simulated meridional wind, vertical velocity, and potential temperature across station A and Mt. Nagi (see Fig. 5) at 0200, 0800, and 1600 UTC 21 August 2001.

At 0200 UTC, several hours before the peak of the Hirodo-kaze, southerlies were present in the upper and middle troposphere and northerlies were present in the lower troposphere (Fig. 7a). Wind speeds at the crest of Mt. Nagi were 10 m s^{-1}. Ascent occurred along the northern (windward) slope of Mt. Nagi and weak descent occurred from 650 hPa down to the surface along the southern lee slope of Mt. Nagi, indicating a downslope wind (Fig. 7b). The region of descent extended far to the lee of Mt. Nagi, but mountain waves were not clearly present in the lee of Mt. Nagi. Thus, although isentropes shifted downward in the lee of Mt. Nagi, a subsequent upward shift in the isentropes to the lee linked to mountain waves was not conspicuous (Fig. 7c).

At 0800 UTC, as the Hirodo-kaze occurred at station A, upper- and middle-tropospheric southerlies persisted as lower-tropospheric northerlies became quite strong (Fig. 8a): wind speeds at the crest of Mt. Nagi exceeded 30 m s^{-1}. Downslope winds developed along the lee slope of Mt. Nagi (Fig. 8b). Maximum descent exceeded 6 m s^{-1}. Isentropes shift downward in the lee of Mt. Nagi until they reached the lower troposphere, and they extended leeward in the lower troposphere over the base of Mt. Nagi (Fig. 8c). The region of strong winds exceeding 30 m s^{-1} extended leeward far from Mt. Nagi. Weak ascent at 35.0°N was related to the topography. These simulation results suggested that during a Hirodo-kaze, strong downslope winds develop along the lee slope of Mt. Nagi and the strong horizon-

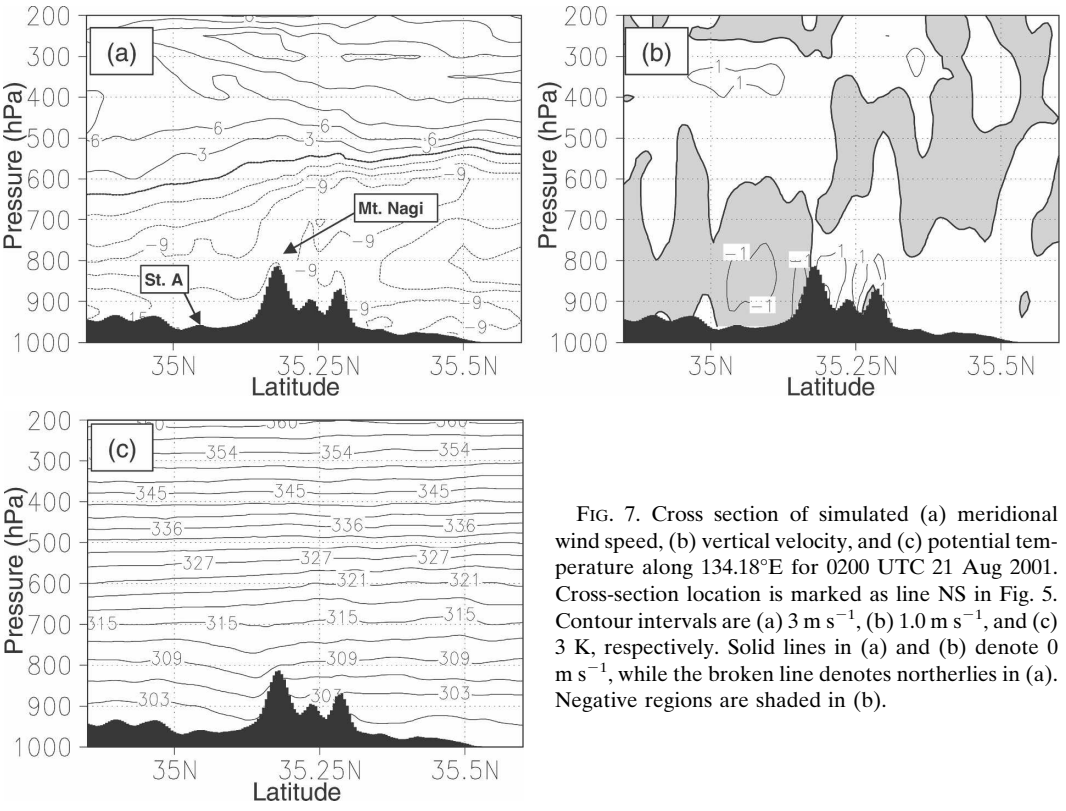

FIG. 7. Cross section of simulated (a) meridional wind speed, (b) vertical velocity, and (c) potential temperature along 134.18°E for 0200 UTC 21 Aug 2001. Cross-section location is marked as line NS in Fig. 5. Contour intervals are (a) 3 m s^{-1}, (b) 1.0 m s^{-1}, and (c) 3 K, respectively. Solid lines in (a) and (b) denote 0 m s^{-1}, while the broken line denotes northerlies in (a). Negative regions are shaded in (b).

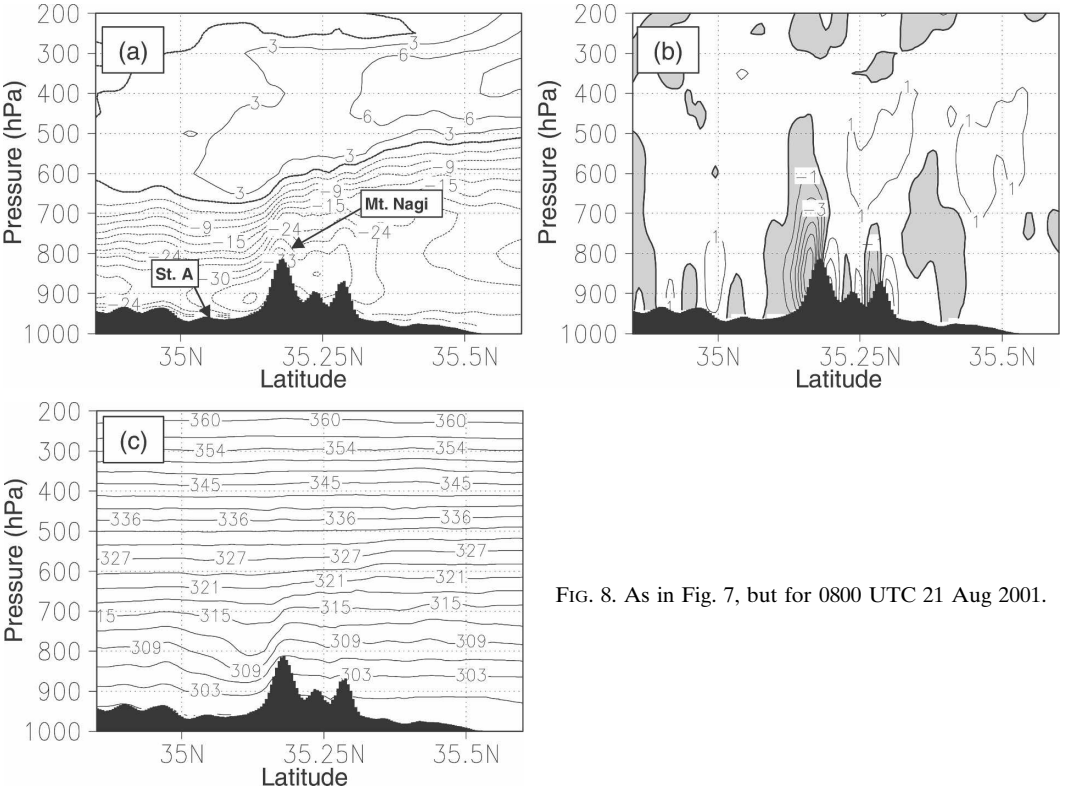

FIG. 8. As in Fig. 7, but for 0800 UTC 21 Aug 2001.

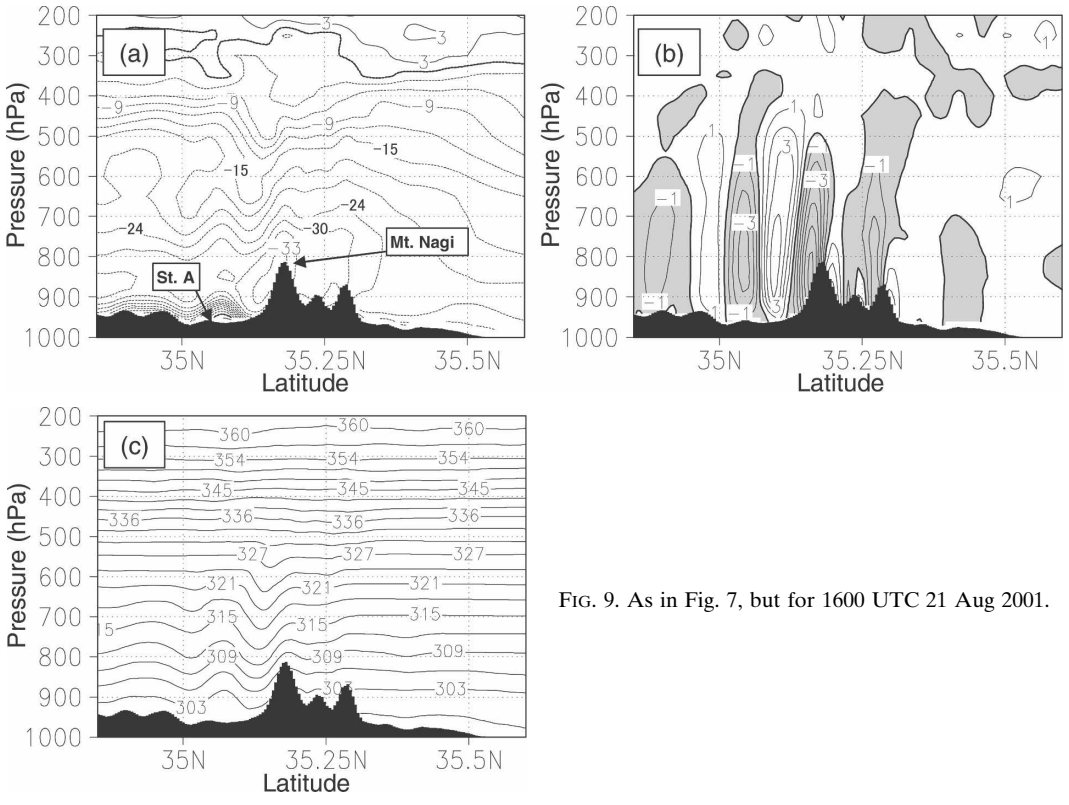

FIG. 9. As in Fig. 7, but for 1600 UTC 21 Aug 2001.

tal winds accompanying the severe downslope winds extend far to the lee of Mt. Nagi.

By 1600 UTC, the Hirodo-kaze had ceased at station A, and middle-tropospheric southerlies changed to northerlies. At the same time, lower-tropospheric northerlies remained strong (Fig. 9a): wind speeds at the crest of Mt. Nagi remained above 30 m s^{-1}. Strong northerlies in the lower troposphere allowed severe downslope winds to persist along the lee slope of Mt. Nagi (Fig. 9b). These severe downslope winds were accompanied by a wavelike vertical circulation in the lee of Mt. Nagi. Mountain waves were also recognized by the rapid downward and subsequent upward shifts in the isentropes (Fig. 9c). The mountain waves dominated in the layer between 600 hPa and the surface. Subsequent ascent at 35.1°N weakened the horizontal winds, forcing a windward retreat of the strong wind region that extended to the lee of Mt. Nagi. These results suggest that after the cessation of a Hirodo-kaze, distinct mountain waves dominate in the lee of Mt. Nagi.

Characteristics of the mountain wave in the lee of Mt. Nagi changed at about 1200 UTC. This temporal change forced the behavior of the Hirodo-kaze. Figure 10 shows time–latitude sections of vertical velocity at 700 hPa and surface meridional wind. Downslope winds, manifested as a strong descent, appeared at 35.15°N between 0400 and 2100 UTC (Fig. 10a). The region of northerly surface winds exceeding 15 m s^{-1} extended southward (leeward) from 0400 to 0900 UTC (Fig. 10b), and subsequently retreated northward (windward) from 0900 to 1200 UTC. Between 0600 and 1200 UTC, the region of strong winds overlapped the location of station A at 35.11°N. This was the peak of the Hirodo-kaze.

After 1200 UTC, steady ascent at 35.09° and 34.98°N and steady descent at 35.03°N persisted in the lee of the downslope winds, indicating distinct mountain waves in the lee of Mt. Nagi (Fig. 10a). Strong surface winds were limited to the region between the downslope winds over Mt. Nagi and subsequent ascent at 35.09°N (Fig. 10b). The subsequent ascent was located windward of station A during this period; therefore, surface wind speeds at station A were weak. This weakness corresponded to the cessation of the Hirodo-kaze. Southerly surface winds appeared in the lee of the subsequent ascent; these winds were consistent with the southerlies at station A after the Hirodo-kaze ceased (Figs. 4 and 6). In the shallow layer below 900 hPa over station A (Fig. 9a), there is the reversal of the horizontal wind with height between the ascent and subsequent descent of a lee wave, characteristic of mountain-wave-

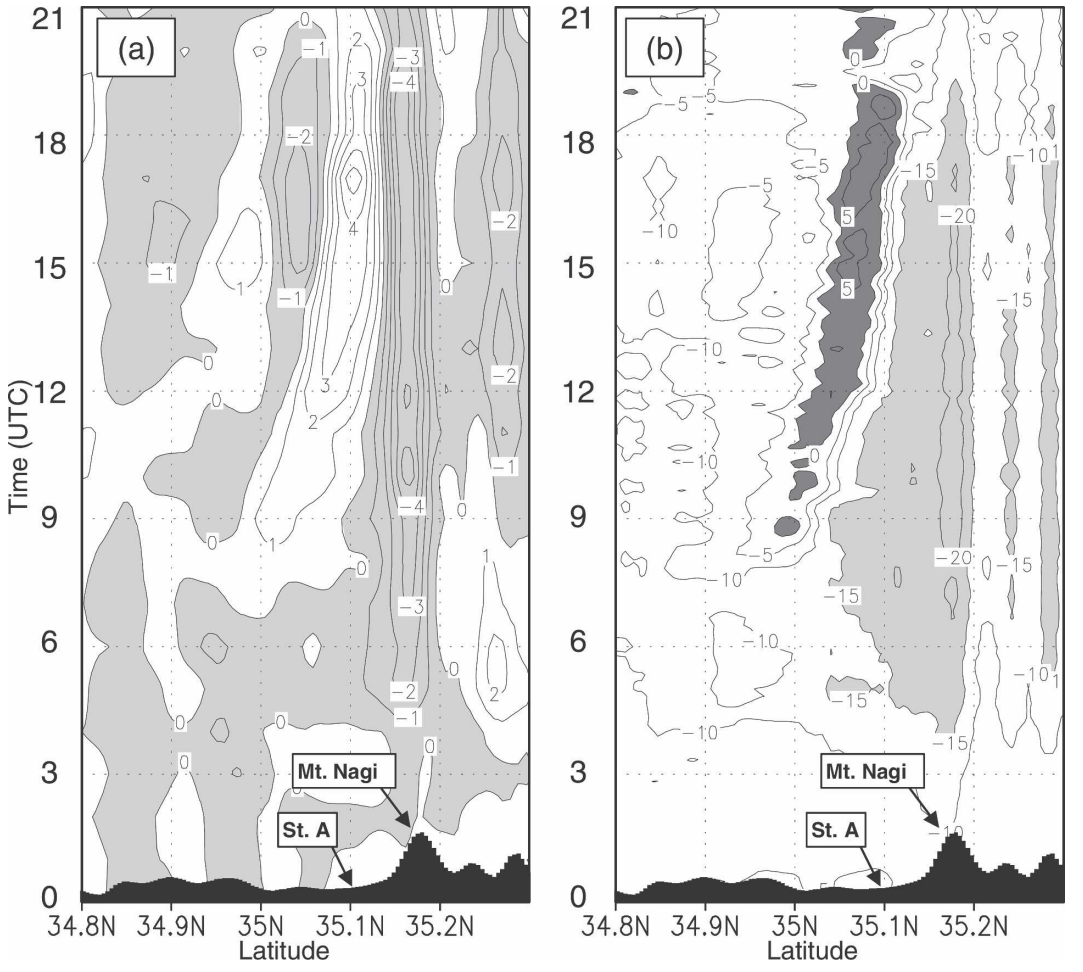

FIG. 10. Time–latitude section of (a) simulated vertical velocity at 700 hPa (contour interval is 1 m s^{-1} and descent is shaded) and (b) meridional surface wind speed (contour interval is 5 m s^{-1}, speeds greater than 15 m s^{-1} are lightly shaded, and southerlies are heavily shaded) along 134.18°E from 0000 to 2100 UTC 21 Aug 2001. Cross-section location is marked as line NS in Fig. 5. The solid shaded region at the bottom of both figures denotes the terrain.

induced rotors (e.g., Doyle and Durran 2002), so that southerly surface winds are regarded as the reversal flow at the base of the mountain-wave-induced rotor.

Changes in the characteristics of mountain waves in the lee of Mt. Nagi are primarily attributed to temporal changes in the large-scale environmental winds due to the movement of Pabuk. Figure 11 shows time series of several quantities averaged in the region surrounding station A (35.0°–35.5°N, 134.0°–134.5°E). Until 0300 UTC, as Pabuk moved over the sea far from the Kii peninsula (Fig. 2), east-northeasterlies prevailed in the lower troposphere and east-southeasterlies prevailed in the upper and middle troposphere (Fig. 11a). As Pabuk approached the Kii peninsula during 0300 and 0900 UTC, lower-tropospheric northerlies strengthened (Fig. 11b). The acceleration of the northerlies forced by the approach of Pabuk caused a leeward extension of the strong wind region (Fig. 10b). On the other hand, middle-tropospheric easterlies continued until 1200 UTC (Fig. 11a), as part of the cyclonic circulation in the northern part of Pabuk (not shown). At 0900 UTC, the middle-tropospheric easterlies started to change to northerlies as Pabuk moved northeast away from Mt. Nagi. Changes in middle-tropospheric winds from southerly to northerly during 0900 and 1200 UTC (Fig. 11b) are related to the changes in the characteristics of mountain waves in the lee of Mt. Nagi. Large-scale environmental winds during the occurrence of the Hirodo-kaze were characterized by strong lower-tropospheric northerlies and middle-tropospheric southerlies.

Throughout the simulation, a continuous stable layer prevailed in the middle and lower troposphere (not shown). This stable layer allowed for the propagation

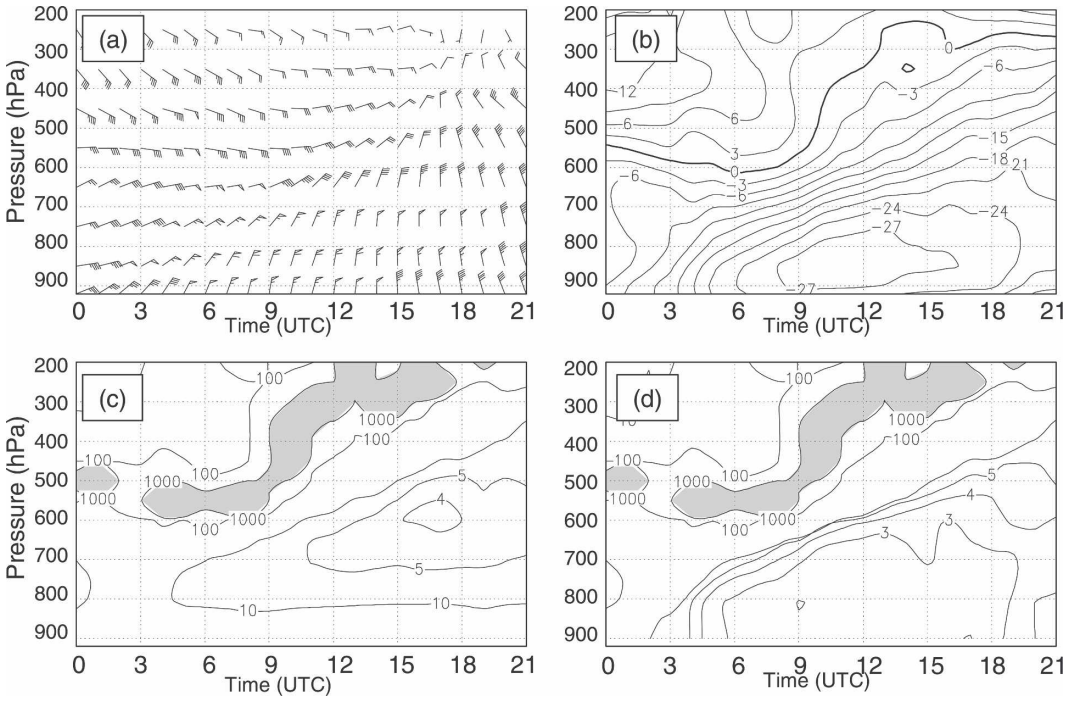

FIG. 11. Time series of simulated (a) horizontal wind, (b) meridional wind speed, (c) Scorer parameter l^2, and (d) first term of Scorer parameter l^2 over the averaged region surrounding station A (35.0°–35.5°N, 134.0°–134.5°E) from 0000 to 2100 UTC 21 Aug 2001. A full wind barb in (a) represents 5 m s^{-1}. Contour intervals are (b) 3 m s^{-1} and (c), (d) $\times 10^{-7}$ m^{-2}. The solid line in (b) represents 0.0 m s^{-1}. Regions higher than 1.0×10^{-4} m^{-2} in (c), (d) are shaded.

of gravity waves over the region. There is, however, no drastic change in the atmospheric static stability during the occurrence of the Hirodo-kaze. Therefore the behavior of the Hirodo-kaze is not affected by the changes in atmospheric static stability.

4. Discussion

Our simulated results reproduced the behavior of the Hirodo-kaze as a temporal change in large-scale environmental winds. The simulation results include the following. Severe downslope winds developed along the lee slope of Mt. Nagi and a region of strong winds accompanying the severe downslope winds extended far to the lee of Mt. Nagi as the Hirodo-kaze occurred (Fig. 8). Distinct mountain waves dominated in the lee of Mt. Nagi after the Hirodo-kaze ceased (Fig. 9).

Durran and Klemp (1982) used a numerical simulation to investigate a case in which the Scorer parameter l^2 decreased with height. The results of their simulations show that a trapped lee wave was caused by partial downward reflection of vertically propagating waves, producing large-amplitude mountain waves in the lee of the mountain. A similar situation arose in our study. Figure 11c shows the Scorer parameter l^2 averaged in the region surrounding station A. The Scorer parameter l^2 is defined as

$$l^2 = \frac{N^2}{\overline{U}^2} - \frac{1}{\overline{U}}\frac{d^2\overline{U}}{dz^2}, \tag{1}$$

where N is the Brunt–Väisälä frequency and $\overline{U}$ is the meridional wind speed. Between 1200 and 2100 UTC, the Scorer parameter l^2 decreased with height below the 600-hPa level, mainly because of an increase in the curvature of the meridional wind speed rather than because of the first term of the Scorer parameter l^2 (Fig. 11d). During this time, distinct mountain waves occurred in the layers below the 600-hPa level in the lee of Mt. Nagi (Fig. 9). The simulated mountain waves had no tilt, a characteristic of trapped lee waves (Durran 1986b). The distinct mountain waves in the lee of Mt. Nagi after 1200 UTC (Fig. 9) were consistent with trapped lee waves for which the Scorer parameter l^2 decreased with height.

Smith's (1985) theory predicts that transitional flow causes strong downslope winds beneath a well-mixed stagnant layer. According to this theory, conditions above the stagnant layer are such that mountain waves are negligible above the stagnant layer. The layer above

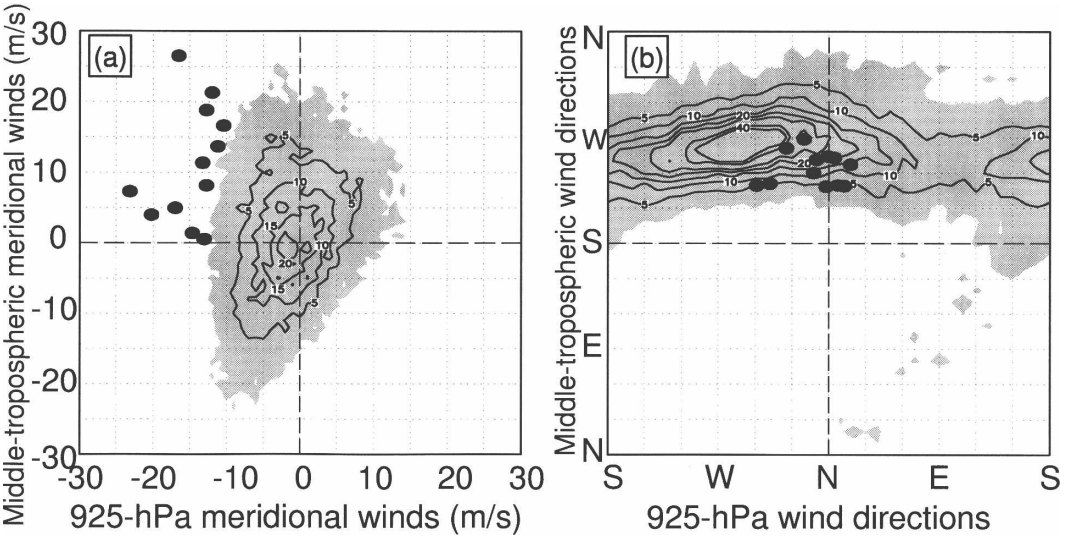

FIG. 12. Frequency distribution of 6-hourly (a) meridional wind speeds and (b) wind directions in the lower troposphere (925 hPa) and middle troposphere (average from 500 to 400 hPa) at grid point 35°N, 135°E. Wind data were obtained from the reanalysis data (ERA-40) between 1989 and 2001. Frequency is counted at each (a) 1 m s^{-1} and (b) 10° intervals. The contour interval is 5 days $(13\ yr)^{-1}$. Regions having >1 day $(13\ yr)^{-1}$ are shaded. Closed circles represent Hirodo-kaze events.

the stagnant layer is therefore consistent with the presence of a critical layer. During the Hirodo-kaze between 0400 and 1200 UTC, a layer in which the Scorer parameter l^2 is infinite existed between 600 and 300 hPa (Fig. 11c)—this layer is affected by the first term of the Scorer parameter (Fig. 11d) and corresponds to the critical layer. This critical layer is present in environmental conditions characterized by middle-tropospheric southerlies and lower-tropospheric northerlies, that is, mean-state critical layer (e.g., Clark and Peltier 1984; Tomine 1984, 1987; Kimura 1992). Below the mean-state critical layer, isentropes began to descend over the crest of Mt. Nagi and continued descending until the flow reached the base of Mt. Nagi (Fig. 8), resembling transitional flow (Smith 1985). The downslope winds that developed were therefore comparable to the severe downslope winds in transitional flow.

Durran and Klemp (1987) studied the relationship between transitional flow and critical-layer height using results from numerical experiments in which the height of a preexisting critical layer in the mean flow and the mountain both varied. Behavior of the transitional flow depended on the height of the critical layer. For the case of Hirodo-kaze, between 0900 and 1200 UTC, the retreat of the region of strong surface winds (Fig. 10b) was related to the weakening transitional flow, which was a response to the change in critical-layer height from 5 to 10 km (Fig. 11c). After 1200 UTC, the critical-layer height was above 10 km, and transitional flow was not clear. Instead, mountain waves related to trapped lee waves dominated, for which the Scorer parameter l^2 decreased with height (Fig. 11c).

The region of strong surface winds extended windward between 0400 and 0900 UTC, the time when the Hirodo-kaze developed (Fig. 10b). The leeward movement of the leading edge of the region resulted from an increase in the lower-troposphere northerlies caused by the approaching Pabuk. In the case of the Yamaji-kaze, the leading edge of the region of strong surface winds, "the Yamaji-kaze front," also moves leeward as the environmental wind increases (Saito and Ikawa 1991). This leeward movement of the region of strong winds caused by increases in environmental winds is similar for both Yamaji-kaze and Hirodo-kaze.

Environmental conditions favorable for the occurrence of a Hirodo-kaze are characterized by strong northerlies in the lower troposphere beneath southerlies in the middle troposphere. Favorable environmental conditions such as these occur over Mt. Nagi when an intense cyclone exists over the sea southwest of the Kii peninsula. Figure 12a presents the frequency of such a configuration of lower- and middle-troposphere meridional winds at the grid point (35°N, 135°E) near Mt. Nagi (35.1°N, 134.2°E) between 1989 and 2001. Data for this plot were obtained from the reanalysis data (ERA-40). According to the several reports of the Okayama meteorological station, 12 Hirodo-kaze events occurred during this period (Nakamura et al. 2002). During these events, strong lower-tropospheric

northerlies exceeding 10 m s^{-1} were overlain by middle-tropospheric southerlies. The configuration described above occurred only during Hirodo-kaze events in the 13 yr. Strong lower-tropospheric northerlies sometimes occurred in winter, but concomitant overlying middle-tropospheric southerlies were not present. Strong lower-tropospheric northerlies were seldom recorded in summer except within an intense cyclone. Favorable environmental conditions occurred only as intense cyclones passed offshore near the Kii peninsula. Thus, intense cyclones that move over the sea southwest of the Kii peninsula produce the favorable environmental conditions that support the occurrence of Hirodo-kaze.

It seems that the shape of mountain range north of Mt. Nagi (see Fig. 1) is favorable for the occurrence of a downslope wind in the case of lower-tropospheric north-northeasterlies rather than north-northwesterlies. Figure 12b shows the frequency distribution of wind directions taken from the same date as in Fig. 12a. The difference in the occurrence of Hirodo-kaze events between north-northeasterly and north-northwesterly winds at the 925-hPa level is not clear. It is noted that the results using wind directions at other lower levels are essentially the same as those using this level. It is difficult to discuss statistically the response of Hirodo-kaze to wind direction as affected by the topography, using ERA-40 with coarse spatial and temporal resolution. Such an examination on an effect of three-dimensional topography to the response of Hirodo-kaze behavior could be considered for future study.

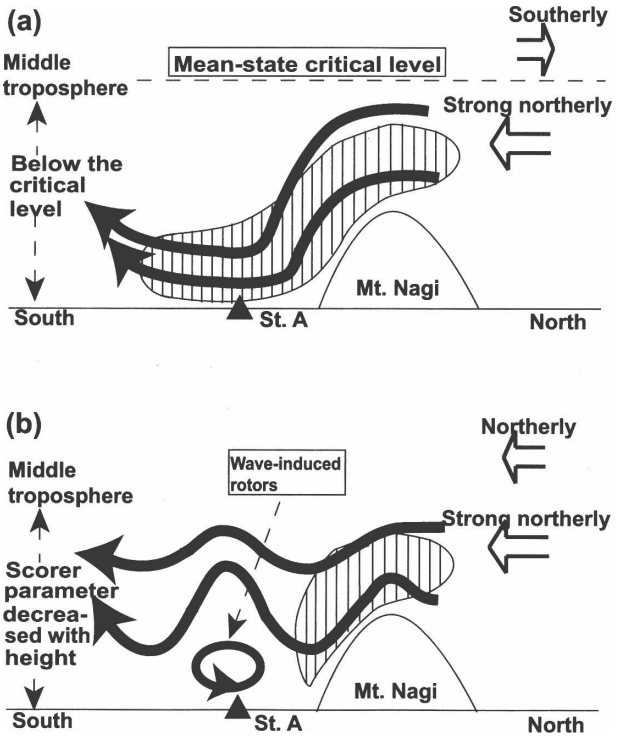

FIG. 13. Schematic cross section of mountain waves through station A and Mt. Nagi for periods of (a) occurrence and (b) cessation of the Hirodo-kaze. Solid arrows indicate streamlines, while open arrows indicate the environmental winds in the middle and lower troposphere. The stippled area indicates a region of strong winds.

5. Summary

A mesoscale numerical model was used to simulate a Hirodo-kaze event that occurred in association with Typhoon Pabuk. The model successfully reproduced the major features of the observed Hirodo-kaze. Figure 13 illustrates the mechanisms controlling the development of the Hirodo-kaze. During a Hirodo-kaze, a mean-state critical layer exists in the middle troposphere (Fig. 13a). Severe downslope winds in the transitional flow develop along the lee slope of Mt. Nagi. The Hirodo-kaze is closely linked to the strong wind region accompanying the severe downslope winds.

After the cessation of the Hirodo-kaze, distinct mountain waves dominate in the lower troposphere where the Scorer parameter l^2 decreases with height (Fig. 13b). The region of strong winds retreats windward as the Hirodo-kaze ceases, although winds at the crest of Mt. Nagi remained strong. The southerly surface winds, a reversal flow at the base of the mountain-wave-induced rotor, appear at station A. Temporal changes in the characteristics of mountain waves in the lee of Mt. Nagi are primarily attributed to changes in the large-scale environmental winds due to the movement of the intense cyclone.

Environmental conditions favorable for the occurrence of the Hirodo-kaze include strong northerlies in the lower troposphere overlain by southerlies in the middle troposphere. These favorable conditions occur only as an intense cyclone moves over the sea southwest of the Kii peninsula. The intense cyclone that moves over the sea southwest of the Kii peninsula thus creates favorable environmental conditions that support the occurrence of the Hirodo-kaze.

The actual structure of a Hirodo-kaze may be more complicated. We used only surface observations to detected Hirodo-kaze. High-resolution radar data are required to detect and characterize mesoscale atmospheric structures accompanying the Hirodo-kaze. Such data will also enhance our ability to predict Hirodo-kaze and lead to a better understanding of strong local-scale winds.

Acknowledgments. We thank Prof. O. Tsukamoto and K. Moritou for their thoughtful comments and for

providing observational data. Thanks are also extended to the staff and students at Okayama University and the Okayama meteorological station for their help and encouragement. Many thanks to Drs. T. Satomura, F. Kimura, M. D. Yamanaka, K. Yasunaga, K. Otsuka, and H. Ueda for fruitful discussions, comments, and criticisms. The authors are grateful for the efforts of many scientists at both PSU and NCAR in maintaining the MM5 and acknowledge the Meteorological Research Institute and Japan Meteorological Agency for supplying meteorological data.

REFERENCES

Anthes, R., E.-Y. Hsie, and Y.-H. Kuo, 1987: Description of the Penn State/NCAR Mesoscale Model version 4 (MM4). NCAR Tech. Note NCAR/TN–282+STR, 66 pp. [Available from NCAR Publications Office, P.O. Box 3000, Boulder, CO 80307-3000.]

Clark, T. L., and W. R. Peltier, 1977: On the evolution and stability of finite-amplitude mountain waves. *J. Atmos. Sci.,* **34,** 1715–1730.

——, and ——, 1984: Critical level reflection and the resonant growth of nonlinear mountain waves. *J. Atmos. Sci.,* **41,** 3122–3134.

Doyle, J. D., and D. R. Durran, 2002: The dynamics of mountain-wave-induced rotors. *J. Atmos. Sci.,* **59,** 186–201.

——, and R. B. Smith, 2003: Mountain waves over the Hohe Tauern: Influence of upstream diabatic effects. *Quart. J. Roy. Meteor. Soc.,* **129,** 799–823.

——, and Coauthors, 2000: An intercomparison of model-predicted wave breaking for the 11 January 1972 Boulder windstorm. *Mon. Wea. Rev.,* **128,** 901–914.

Dudhia, J., 1989: Numerical study of convection observed during the Winter Monsoon Experiment using a mesoscale two-dimensional model. *J. Atmos. Sci.,* **46,** 3077–3107.

——, 1993: A nonhydrostatic version of the Penn State–NCAR Mesoscale Model: Validation tests and simulation of an Atlantic cyclone and cold front. *Mon. Wea. Rev.,* **121,** 1493–1513.

Durran, D. R., 1986a: Another look at downslope windstorms. Part I: The development of analogs to supercritical flow in an infinitely deep, continuously stratified fluid. *J. Atmos. Sci.,* **43,** 2527–2543.

——, 1986b: Mountain waves. *Mesoscale Meteorology and Forecasting,* P. S. Ray, Ed., Amer. Meteor. Soc., 472–492.

——, and J. B. Klemp, 1982: The effects of moisture on trapped mountain lee waves. *J. Atmos. Sci.,* **39,** 2490–2506.

——, and ——, 1987: Another look at downslope winds. Part II: Nonlinear amplification beneath wave-overturning layers. *J. Atmos. Sci.,* **44,** 3402–3412.

Furger, M., P. Drobinski, A. S. H. Prévôt, R. O. Weber, W. K. Graber, and B. Neininger, 2001: Comparison of horizontal and vertical scintillometer crosswinds during strong foehn with lidar and aircraft measurements. *J. Atmos. Oceanic Technol.,* **18,** 1975–1988.

Grell, G. A., J. Dudhia, and D. R. Stauffer, 1995: A description of the fifth-generation Penn State/NCAR Mesoscale Model (MM5). NCAR Tech. Note NCAR/TN-398+STR, 138 pp. [Available from NCAR Publications Office, P.O. Box 3000, Boulder, CO 80307-3000.]

Hong, S.-Y., and H.-L. Pan, 1996: Nonlocal boundary layer vertical diffusion in a medium-range forecast model. *Mon. Wea. Rev.,* **124,** 2322–2339.

Ikawa, M., and Y. Nagasawa, 1989: A numerical study of a dynamically induced foehn observed in the Abashiri-Ohmu area. *J. Meteor. Soc. Japan,* **67,** 429–458.

Jackson, P. L., and D. G. Steyn, 1994: Gap winds in a fjord. Part I: Observations and numerical simulation. *Mon. Wea. Rev.,* **122,** 2645–2665.

Jiang, Q., and J. D. Doyle, 2005: Wave breaking induced surface wakes and jets observed during a bora event. *Geophys. Res. Lett.,* **32,** L17807, doi:10.1029/2005GL022398.

——, ——, and R. B. Smith, 2006: Interaction between trapped waves and boundary layers. *J. Atmos. Sci.,* **63,** 617–633.

——, ——, S. Wang, and R. B. Smith, 2007: On boundary layer separation in the lee of mesoscale topography. *J. Atmos. Sci.,* **64,** 401–420.

Kimura, F., 1992: Local circulation: Guidance to meteorology (in Japanese). *Tenki,* **39,** 377–383.

Klemp, J. B., and D. K. Lilly, 1975: The dynamics of wave-induced downslope winds. *J. Atmos. Sci.,* **32,** 320–339.

Lilly, D. K., and E. J. Zipser, 1972: The front range windstorm of 11 January 1972—A meteorological narrative. *Weatherwise,* **25,** 56–63.

Long, R. R., 1954: Some aspects of the flow of stratified fluids. II. Experiments with a two-fluid system. *Tellus,* **6,** 97–115.

Nakamura, M., and Coauthors, 2002: Experimental study of the downslope wind "Hiroto-Kaze" occurrence at Mt. Nagi (in Japanese). *Tenki,* **49,** 129–139.

Peltier, W. R., and T. L. Clark, 1979: The evolution and stability of finite-amplitude mountain waves. Part II: Surface wave drag and severe downslope windstorms. *J. Atmos. Sci.,* **36,** 1498–1529.

Queney, P., G. Corby, N. Gerbier, H. Koschmieder, and J. Zierep, 1960: The airflow over mountains. WMO Tech. Note 34, 135 pp.

Reed, R. J., 1981: A case study of a bora-like windstorm in western Washington. *Mon. Wea. Rev.,* **109,** 2383–2393.

Sahashi, K., 1988: A roll accompanied by HIROTO-KAZE (in Japanese). *Tenki,* **35,** 497–499.

——, 1993: *Weather of Okayama Prefecture (in Japanese).* Sanyo Newspaper, 224 pp.

Saito, K., 1992: Shallow water flow having a lee hydraulic jump over a mountain range in a channel of variable width. *J. Meteor. Soc. Japan,* **70,** 775–782.

——, 1993: A numerical study of the local downslope wind "Yamaji-kaze" in Japan. Part 2: Non-linear aspect of the 3-D flow over a mountain range with a col. *J. Meteor. Soc. Japan,* **71,** 247–271.

——, 1994: A numerical study of the local downslope wind "Yamaji-kaze" in Japan. Part 3: Numerical simulation of the 27 September 1991 windstorm with a non-hydrostatic multi-nested model. *J. Meteor. Soc. Japan,* **72,** 301–329.

——, and M. Ikawa, 1991: A numerical study of the local downslope wind "Yamaji-kaze" in Japan. *J. Meteor. Soc. Japan,* **69,** 31–56.

Smith, R. B., 1985: On severe downslope winds. *J. Atmos. Sci.,* **42,** 2597–2603.

——, 1987: Aerial observations of the Yugoslavian bora. *J. Atmos. Sci.,* **44,** 269–297.

Tomine, K., 1984: A numerical study on local depressions in the gravity wave regime. *J. Meteor. Soc. Japan,* **62,** 215–223.

——, 1987: A supplementary study of simulations of mountain wave critical level interactions. *J. Meteor. Soc. Japan,* **65,** 145–148.

Vosper, S. B., 2004: Inversion effects on mountain lee waves. *Quart. J. Roy. Meteor. Soc.,* **130,** 1723–1748.

——, P. F. Sheridan, and A. R. Brown, 2006: Flow separation and rotor formation beneath two-dimensional trapped lee waves. *Quart. J. Roy. Meteor. Soc.,* **132,** 2415–2438.

Yoshino, M., 1986: *Small Climate* (in Japanese). New ed. Chijin Shokan, 298 pp.

Zängl, G., 2002: Stratified flow over a mountain with a gap: Linear theory and numerical simulations. *Quart. J. Roy. Meteor. Soc.,* **128,** 927–949.